ISSN 0915-633X

NATIONAL INSTITUTE FOR FUSION SCIENCE

A Mechanism of Collisionless Magnetic Reconnection

M. Tanaka

(Received – Feb. 23, 1994)

NIFS-274 Mar. 1994

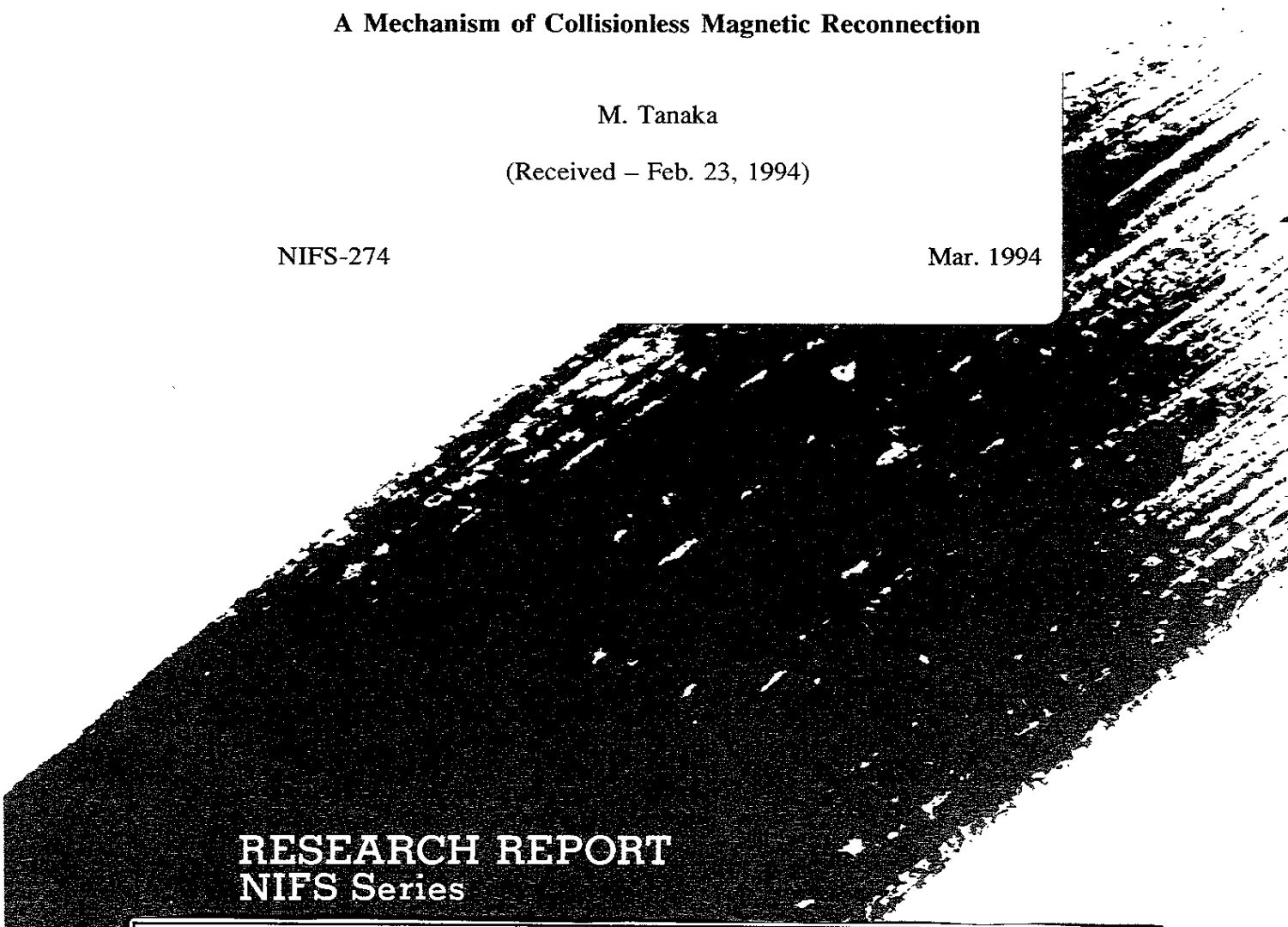

RESEARCH REPORT
NIFS Series

NAGOYA, JAPAN

A Mechanism of Collisionless Magnetic Reconnection

Motohiko Tanaka

National Institute for Fusion Science

Nagoya 464-01, Japan

Abstract

Forced reconnection in a collisionless magnetized plasma is studied using an implicit particle simulation. A coalescence of magnetic islands induces the electric field E_t at the x-point via the displacement current. A quasi-steady reconnection is achieved with $E_t \neq 0$, the poloidal electric field E_p generated by electrostatic shielding, and the current J_t continuously removed via the $E_p \times B$ plasma convection. Transit acceleration of electrons by unshielded parallel electric field $E_\parallel \cong E_t$ at the x-point yields the Ohm's law $E_t \cong \eta_{eq} J_t$ with η_{eq} the inertia (kinetic) resistivity.

Keywords: Magnetic reconnection, anomalous dissipation,
electron inertia, implicit particle simulation.

1. Introduction

Magnetic reconnection is believed to play an important role in changing topology of magnetic field and converting its energy to plasma directed and thermal energies in fusion and astrophysical plasmas. Global studies of magnetic reconnection are based on the magnetohydrodynamic (MHD) equations which are combined with dissipation of plasma current. However, an origin of anomalous dissipation that should arise from non-Coulomb collisional processes has remained a key question of plasma physics for many years.

An importance of electron inertia for the collisionless reconnection was noticed and studied in the MHD framework[1] and in the kinetic viewpoint with electromagnetic fields assumed[2]. Later studies focused on the internal m=1 kink and tearing modes where they adopted the MHD (fluid) equations and the generalized Ohm's law with electron inertia current[3–6]. In these studies, however, the toroidal current became quite peaked and non-zero resistivity was required to remove singularity at the x-point and split up the magnetic field. Nonlinear growth of magnetic island was studied analytically[7–10] and by particle simulations[11,12]. But, the full kinetic process of collisionless reconnection still remains unclear.

For elucidating the mechanism of collisionless reconnection from a fundamental kinetic viewpoint, we study in this Letter a coalescence of magnetic islands by means of $2\frac{1}{2}$-D electromagnetic, implicit particle simulation (macro-particle, HIDENEK) code[13]. In this study, a plasma is magnetized by the toroidal magnetic field, as is the case with high-temperature, non-resistive plasmas found in magnetic fusion devices[14,15] and the solar corona[16]. The simulation is done in the magnetized ion regime; for the TFTR parameters[14] the ion gyroradius becomes $\rho_i \cong 4c/\omega_{pe}$. We use the electron inertia length c/ω_{pe} as the unit of length. It is mentioned that coalescence of magnetic islands leads to the forced (self-driven) reconnection without an external electric field, $E_t^{(0)} = 0$. This makes it easier to identify the generation mechanism of the toroidal electric field

in the diffusion layer.

An advantage of the implicit particle simulation[13] compared with the conventional ones is realization of large time-and-space scales, $L \geq c/\omega_{pe}$ and $\omega_{pe}\tau \gg 1$, including electron dynamics. Maxwell equations with the displacement current,

$$\partial \mathbf{E}/\partial t = c\nabla \times \mathbf{B} - 4\pi \mathbf{J}, \quad \nabla \cdot \mathbf{E} = 4\pi\rho, \tag{1}$$

$$\partial \mathbf{B}/\partial t = -c\nabla \times \mathbf{E}, \quad \nabla \cdot \mathbf{B} = 0, \tag{2}$$

are solved using time-decentering technique that filters out high frequency components of the electromagnetic oscillations, where $\mathbf{E}$ and $\mathbf{B}$ are the electric and magnetic fields, respectively. The Newton-Lorentz equations of motion without a collision term,

$$d\mathbf{x}_j/dt = \mathbf{v}_j, \tag{3}$$

$$d\mathbf{v}_j/dt = (e/m_i)[\mathbf{E} + (\mathbf{v}_j/c) \times \mathbf{B}], \tag{4}$$

are solved for the positions $\mathbf{x}_j$ and velocities $\mathbf{v}_j$ of each particle ion. For the electrons, the drift-kinetic equations,

$$d\mathbf{x}_j/dt = [v_{\|j}\mathbf{b} + \mathbf{v}_{\perp j}], \tag{5}$$

$$m_e dv_{\|j}/dt = (-e)E_{\|} - \mu_j \nabla_{\|} B \tag{6}$$

are adopted, where $v_{\|j}$, $\mathbf{v}_{\perp j}$ are the parallel and perpendicular (guiding-center) velocities, respectively, $\mathbf{b}$ the unit vector along the magnetic field, and μ_j the magnetic moment. In order to have a good spatial resolution of the "diffusion layer" which is formed around $x \cong \frac{1}{2}L_x$, spatially-fixed uneven meshes are adopted in the x-direction. Furthermore, to keep the particle fluctuations in a low level, one giant particle is split into a few small particles with the (q_j/m_j) ratio fixed when it has entered the fine-mesh region located around the center of the system. On the other hand, small particles once split are not coalesced to the original size particles to avoid physics ambiguity in the present study.

2. Simulation Results

To set up a simulation, a charge-neutral plasma with the same number of ions and electrons (64 ions/cell) is loaded homogeneously in a doubly-periodic Cartesian system of two dimensions. The system size is $L_x = 400c/\omega_{pe}$ and $L_z = 300c/\omega_{pe}$ with 320×72 cells. The grid interval is $\Delta x \cong 0.55c/\omega_{pe}$ for the central part (107 cells) and $\Delta x \cong 1.6c/\omega_{pe}$ for the rest, and $\Delta z \cong 4.1c/\omega_{pe}$ in the z-direction. The particle velocities are generated according to the Boltzmann distribution of given temperatures. The ions residing in two square areas are drifting initially at $V_{di}/c = 0.01$ in the positive y-direction to produce a pair of magnetic islands. All the electrons distributed uniformly in the system are drifting at an equal velocity in the y-direction so that there is no net current. The physical parameters are the mass ratio $m_i/m_e = 100$, the strength of the ambient toroidal (y-direction) magnetic field $\omega_{ce}^{(0)}/\omega_{pe} = 1$, electron beta value $\beta_e = 8\pi n T_e/B^2 = 0.04$, and the temperature ratio $T_i/T_e = 1$. The ion gyroradius becomes $\rho_i \cong 2c/\omega_{pe}$, and the time step is chosen to be $\omega_{pe}\Delta t = 50$.

Figure 1 shows the poloidal magnetic flux function Ψ defined by $\mathbf{B}_p = \nabla \times (\Psi \hat{y})$, and the toroidal component of the ion current $J_y^{(i)}$ at $t/\tau_A = 0$, 1.6 and 3.1. Here, the Alfven time is defined by $\tau_A = \frac{1}{2} d/v_{Ap} \sim 3200\omega_{pe}^{-1}$ with $d = 160c/\omega_{pe}$ the initial distance between the magnetic islands, and $v_{Ap} = B_p^{(0)}/(4\pi m_i n)^{1/2} \sim 0.025c$. (The Alfven time defined by the diffusion layer width is much shorter.) For $t > 0$, the islands get attracted by magnetic force and then squeezed at the contact surface to form an elongated diffusion layer. As will be shown in Fig.2, the magnetic reconnection sets in around $t/\tau_A \cong 1.4$. By this time, the layer width has been narrowed to $L_B \cong 3c/\omega_{pe}$ (half-width) which is comparable to electron inertia length, as will be shown in Fig.4.

Occurrence of magnetic reconnection is detected by measuring the amount of isolated poloidal magnetic flux that is contained in either of the islands. The number of isolated Ψ-contours stays the same for Fig.1(a) and (b), but it decreases between (b) and (c). (The total poloidal magnetic flux is conserved within three percent.) The flux

merging slows down for $t/\tau_A \geq 4$ and approximately a third of the initially isolated flux remains unreconnected, which is consistent with partial reconnection of two flux cores of the same sign helicities[17]. The toroidal current of ions shown in Fig.1 gradually pinches off and its contours become more or less round-shaped in an early time because the initial pressure profile is uniform. As the two islands collide, a substantial amount of negative toroidal current is induced in the gap dividing the islands. The toroidal current which is mostly carried by the electrons reaches a maximum around $t \cong 2\tau_A$. At this time, the negative current occupies the thin elongated (Y-shaped) diffusion layer. But, the intensity and area of the negative current decreases gradually as the flux merging proceeds.

The time histories of the toroidal current J_y and the electric field E_y measured at $x \cong \frac{1}{2}L_x$ are shown in Fig.2 in logarithmic scales (the signs reversed). The toroidal electric field directly relates to magnetic reconnection through the Faraday's law. The toroidal current and electric field are observed to grow exponentially with the growth rate $\gamma\tau_A \sim 2.6$ and saturate around $t \cong 2\tau_A$. Also, the time history of the isolated poloidal magnetic flux is shown in a linear scale. The amount of the isolated flux $\Delta\Psi$ is defined as the difference between the peak flux in the magnetic island (averaged) and that on the separatrix. The isolated flux stays nearly in the same level in the early phase up to $t/\tau_A \cong 1.4$. The flux decreases linearly in time for $t/\tau_A \geq 1.9$ which corresponds to saturation of the toroidal electric field. The observed time-linear flux annihilation in the main phase of reconnection coincides with nearly constant toroidal electric field, $(d\Delta\Psi/dt)_{obs} \cong -1.2\tau_A^{-1}$ whereas the theoretical value becomes $d\Delta\Psi/dt = -c <E_y> \cong -1.3\tau_A^{-1}$. The time-linear flux annihilation is apparently the Sweet-Parker type reconnection[18,19] $\Delta\Psi \propto t$. Moreover, the early nonlinear stage which was identified in the resistive MHD studies[7,9] is short ($1.4 < t/\tau_A < 1.9$). Namely, the full-nonlinear stage starts shortly following the onset of magnetic reconnection.

The two-dimensional snapshots of the electric and magnetic fields, and the ion and

electron currents at $t/\tau_A = 1.6$ are shown in Fig.3. The toroidal electric field in Fig.3(b) takes a negative value in a wide region exactly between the two magnetic islands and continues to cover the same region. It is noted that the spatial extent of the induced toroidal current in Fig.3(d)(e) is much narrower than that of the E_y electric field (explained below). The poloidal electric field displayed in Fig.3(a) is more intense than its toroidal component. This electric field is stationary in time and has a divergence which is better depicted in the electrostatic potential φ ($\mathbf{E}_p = -\nabla\varphi$) of Fig.3(f). Obviously, the charge redistribution has taken place in a quadrupole configuration in the regions outside the diffusion layer; more negative charge accumulates in the first and third quadrants with the origin at the x-point.

In a broad region between the magnetic islands, both a curl of the poloidal magnetic field and the quantity that equals to the displacement current are observed to be negative, $(\nabla \times \mathbf{B})_y$ and $(\nabla \times \mathbf{B})_y - (4\pi/c)J_y < 0$ as shown in Fig.4(a) and (b), respectively, until the saturation of the E_y field. Next, a projection of the poloidal electric field onto the helical magnetic field is seen to have a distinct positive profile with a sharp null hole centered at $x \cong \frac{1}{2}L_x$. The null hole exists because the poloidal electric field vanishes due to symmetry in φ and because the magnetic field is nearly perpendicular to the reconnection plane. Thirdly, the parallel component of the electric field $E_\parallel = E_y b_y - \mathbf{b}\cdot\nabla\varphi$ is found to be small, $E_\parallel \ll E_y$, except in the diffusion layer where $\mathbf{b} = \mathbf{B}/B$.

Thus, it is concluded that the toroidal electric field is induced via the displacement current by imbalance of the magnetic field change and the toroidal plasma current. Also, the quadrupole electrostatic potential is a result of the electron adjustment along the magnetic field to shield the parallel electric field, $E_\parallel \cong 0$. This potential results in the E_z field laterally across the islands in Fig.3(a), and a more intense electric field E_x concentrated in the diffusion layer, pointing downward for $z < \frac{1}{2}L_z$ and upward for $z > \frac{1}{2}L_z$. Here, we note $E_x/E_z \cong l_z/l_x \gg 1$, as the diffusion layer is elongated, i.e.,

its width l_x less than its length l_z. Thirdly, incompletely shielded parallel electric field $E_{\parallel}$ in the diffusion layer produces the negative toroidal current by accelerating light mass electrons, as shown in Fig.2. Thus, the toroidal current is confined to the narrow diffusion layer.

The poloidal component of the plasma current, electric and magnetic fields in the diffusion layer is shown in Fig.5. The ion flow is essentially the same with the ion current ($n_i \cong const.$). The ions flow in vertically almost along the equicontour of the potential φ toward the diffusion layer and are diverted to the lateral direction. A close comparison of Fig.5(a) and (c) reveals that the ion flow is driven by the $E \times B$ drift. In fact, the observed outward velocity $V_z = 0.021c$ ($\sim v_{Ap}$) coincides with $V_{E\times B} \sim 0.022c$ estimated by $\mathbf{E}_p = -\nabla\varphi$. Although both the toroidal and poloidal electric fields contribute to the plasma convection, the poloidal electric field is predominant, $\mathbf{E} \times \mathbf{B} \cong \mathbf{E}_p \times \mathbf{B}_t$ since $E_p \gg E_t$ and $B_t > B_p$. The electron current in Fig.5(b) nearly cancels the ion current in the poloidal plane in the present magnetized case. A slight asymmetric pattern in the electron current, i.e. anti-parallel current penetrating through the diffusion layer, is accounted for by the ∇B drift.

The toroidal current J_y localized in the diffusion layer blocks the incoming plasma and magnetic flux by repulsive force and could impede magnetic reconnection. However, the plasma particles carrying the J_y-current are quickly removed from the diffusion layer at the speed close to the Alfven speed. This is expected to maintain the quasi-steady collisionless reconnection. To prove this point, a special run has been made by artificially reducing the poloidal electric field (E_x, E_z) to 70% of its real value in the diffusion layer, keeping all the other conditions being fixed. In this case, plasma density is observed to pile up in the diffusion layer because the ions and electrons are not efficiently pumped out by the $E_p \times B$ drift. Actually, the reconnection rate still scales linearly in time, but it is drastically suppressed compared with the value shown in Fig.2, i.e., from $(d\Delta\Psi/dt)/\Delta\Psi^{(0)} \sim -0.23\tau_A^{-1}$ to $-0.08\tau_A^{-1}$.

In order to examine the role of the ions in the collisionless reconnection, other runs have been made by changing either the mass ratio $m_i/m_e = 50 \sim 200$ or the ion temperature $T_i/T_e = \frac{1}{9} \sim 9$. The ion gyroradius becomes $\rho_i/L_B \cong 0.2 \sim 2$. But, no appreciable change in the width of the diffusion layer has been observed with the flux reconnection rate scattered in the range $(d\Delta\Psi/dt)/\Delta\Psi^{(0)} \sim -(0.23 - 0.27)\tau_A^{-1}$. This implies that the collisionless "forced" reconnection is governed by the electrons as far as the ions are magnetized, as is different from the case where m=1 tearing mode plays an essential role[20].

3. Mechanism of Collisionless Reconnection

A close inspection of the simulation evidences may lead to the following mechanism of forced reconnection in a collisionless magnetized plasma:

(i) When the magnetic field changes, the toroidal electric field E_y arises only from the displacement current as it is purely electromagnetic in the $2\frac{1}{2}$-D geometry,

$$\partial E_y/\partial t \;=\; c(\nabla \times \mathbf{B})_y \;-\; 4\pi J_y \;\leq\; 0. \tag{7}$$

This non-MHD process directly induces the toroidal electric field at the x-point (the sign is pertinent to the present geometry).

(ii) The imbalance Eq.(7) in the initial stage, which becomes significant in the c/ω_{pe} scales, is attributed to slow plasma response due to finite inertia against magnetic field change. Later, a quasi-steady state with $E_y < 0$ and $\nabla \times \mathbf{B} \cong (4\pi/c)\mathbf{J}$ is maintained by continuous removal of the J_y-current being carried by the $E_p \times B$ convecting particles.

(iii) With the toroidal electric field E_y, magnetic reconnection is inevitable:

$$\partial \mathbf{B}_p/\partial t \;=\; -c\nabla \times (E_y\hat{y}) \neq 0. \tag{8}$$

In the poloidal magnetic flux, $\partial\Psi/\partial t = -cE_y > 0$. This reduces strength of the poloidal magnetic field and forces it to reconnect at the x-point.

A catalytic process in the main stage (ii) is: the parallel electric field $E_{\|} \cong E_y$ at the x-point produces the toroidal current J_y. Outside the diffusion layer, the electrostatic potential φ, hence the poloidal electric field E_p, is generated by electrostatic shielding,

$$E_{\|} = E_y b_y - \mathbf{b} \cdot \nabla \varphi \cong 0. \tag{9}$$

This field is directly responsible for the $E_p \times B$ plasma convection and the removal of the toroidal current. It is mentioned in passing that the present mechanism will also apply to weakly magnetized plasmas with $\rho_i \geq L_B$ since the ions are playing little role, as observed in the simulations.

Coexistence of the toroidal electric field and current in the diffusion layer, which has been confirmed in the present study, supports that the collisionless dissipation in the MHD description is provided by a transit acceleration of the "finite mass" electrons[2]. Since $E_{\|} \cong E_t$, the toroidal current may be written as

$$J_t^{(e)} = (-e) n \delta v_t^{(e)} \cong (ne^2/m_e) E_t \tau_{tr}, \tag{10}$$

where τ_{tr} is an electron transit time through the diffusion layer which is a function of E_p and is determined by a global plasma condition. Substitution of Eq.(10) into the Ampere's law yields the quasi-steady toroidal electric field,

$$E_t \cong (c\tau_{tr}/L_B) B_p/(1 + \omega_{pe}^2 \tau_{tr}^2), \tag{11}$$

where $L_B = (\partial \log B_p/\partial x)^{-1}$. With aid of the Faraday's law, one gets the theoretical width of the diffusion layer as

$$L_B^{(th)} \cong c/\omega_{pe}. \tag{12}$$

A similar result was heuristically obtained[5]. But, it is emphasized that the "kinetic" inertia $d\mathbf{v}_j/dt$ and Eq.(10) are more general than the $dJ_{\|}/dt$ term in the generalized Ohm's law that disappears and yields no dissipation right at the x-point. Therefore,

on the basis of evidences in particle simulation, we obtain the collisionless version of the Ohm's law

$$E_t \cong \eta_{eq} J_t \tag{13}$$

with the equivalent resistivity written as $\eta_{eq} = 4\pi/\omega_{pe}^2 \tau_{tr}$. The reconnection time becomes $\tau \sim (L_B \omega_{pe}/c)^2 \tau_{tr}$ which is much shorter than the collisional time.

4. Summary and Conclusion

It has been shown using the implicit particle simulation method (macro-particle, HIDENEK) that the quasi-steady magnetic reconnection is achieved in collisionless magnetized plasmas. The non-MHD effects such as the displacement current and the electrostatic shielding /unshielding due to parallel electron adjustment have been found to play essential roles in maintaining the reconnection (toroidal) electric field at the x-point. The magnetic flux annihilation has occurred linearly in time like the Sweet-Parker type reconnection. The collisionless Ohm's law with equivalent resistivity has been proven to be provided by transit electron acceleration due to the electric field which remains unshielded in the diffusion layer.

The present study has been done for the magnetized plasma where the toroidal magnetic field is stronger than the poloidal magnetic field, $B_p < B_t$. A series of new simulation has been started for the opposite case with $B_p > B_t$ where the ions are only weakly magnetized. In the new simulation, the electrons are time-advanced using the Newton-Lorentz equations of motion, Eq.(3) and (4). It has been observed that the toroidal electric field E_y is induced in an early stage and maintained in a broad region between the two magnetic islands, which is similar to the magnetized case. Precise results of collisionless magnetic reconnection in the unmagnetized plasma will be reported in the near future.

Finally, a coupling of the collisionless forced reconnection with internal m=1 tearing mode and current-driven instabilities is an important problem to totally understand the kinetic process of magnetic reconnection. The latter study requires a full three-dimensional geometry which seems to be quite challenging.

Acknowledgements

The author gratefully acknowledges valuable discussions with Dr.J.U.Brackbill and Dr.J.Todoroki on the ill-conditioned matrix inversion. He deeply thanks Dr.J.F.Drake, Dr.A.Bhattacharjee, and Dr.H.Narita for stimulating discussions and encouragements.

References

1. B.Coppi, Phys.Fluids, 8, 2273 (1965).
2. T.W.Speicer, Planet.Space Sci., 18, 613 (1970).
3. J.F.Drake, Phys.Fluids, 21, 1777 (1978).
4. J.F.Drake and R.G.Kleva, Phys.Rev.Lett., 66, 1458 (1991).
5. A.Y.Aydemir, Phys.Fluids, B2, 2135 (1990).
6. J.A.Wesson, JET Report P-27 (1990).
7. D.Biskamp and H.Welter, Phys.Rev.Lett., 44, 1069 (1980).
8. F.L.Waelbroeck, Phys.Fluids, B1, 2372 (1989).
9. X.Wang and A.Bhattacharjee, Phys.Fluids, B4, 1795 (1992).
10. M.Ottaviani and F.Porcelli, Phys.Rev.Lett., 71, 3802 (1993).
11. T.Tajima, F.Brunel and J.Sakai, Astrophys.J., 258, L45 (1982).
12. D.W.Hewett, G.E.Francis and L.E.Max, Phys.Rev.Lett., 61, 893 (1988).
13. M.Tanaka, J.Comput.Phys., 107, 124 (1993); ibid., 79, 209 (1988).
14. K.McGuire and TFTR team, Phys.Fluids, B2, 1287 (1990).
15. B.Coppi, S.Migliuolo, F.Pegoraro and F.Porcelli, Phys.Fluids, B2, 927 (1990).
16. E.R.Priest, Solar Magnetohydrodynamics (D.Reidel Publ.Co., Holland, 1982)
17. M.Yamada, Y.Ono, A.Hayakawa, M.Katsurai, and F.W.Perkins, Phys.Rev.Lett., 65, 721 (1990).
18. P.A.Sweet, Nuovo Cimento, 8, 188 (1958).
19. E.N.Parker, Astrophys.J.Suppl., 77, 177 (1963).
20. F.Porcelli, Phys.Rev.Lett., 66, 425 (1991).

Figure Captions

FIG. 1. Snapshots of poloidal magnetic flux function Ψ (top), and the y-component of ion current $J_y^{(i)}$ (bottom) for the times $t/\tau_A =$ (a) 0, (b) 1.6 and (c) 3.1.

FIG. 2. Time histories of toroidal electric field (solid), toroidal current (dashed), and isolated poloidal flux $\Delta\Psi$ contained in either of the islands. The magnetic flux function is normalized as $e\Psi/m_e c^2$.

FIG. 3. (a)(b) Poloidal and toroidal electric fields, respectively, (c) poloidal magnetic field, (d)(e) ion and electron currents, and (f) electrostatic potential φ at $t/\tau_A = 1.6$. The maximum values are (a) 2.1×10^{-2}, (b) 1.9×10^{-3}, (c) 0.23, (d) 0.80, (e) 4.0, and (f) 0.43. (The electromagnetic fields are normalized as $eE/m_e c\omega_{pe}$.)

FIG. 4. (a) Curl of the poloidal magnetic field $(\nabla \times \mathbf{B})_y$, and (b) the quantity that equals to the displacement current, $(\nabla \times \mathbf{B})_y - 4\pi J_y$ at $t/\tau_A = 0.63$.

FIG. 5. Magnified plots of ion and electron currents in (a) and (b), electric and magnetic fields in (c) and (d), respectively, for $t/\tau_A = 1.6$. (vectors are plotted in every other x-grid point).

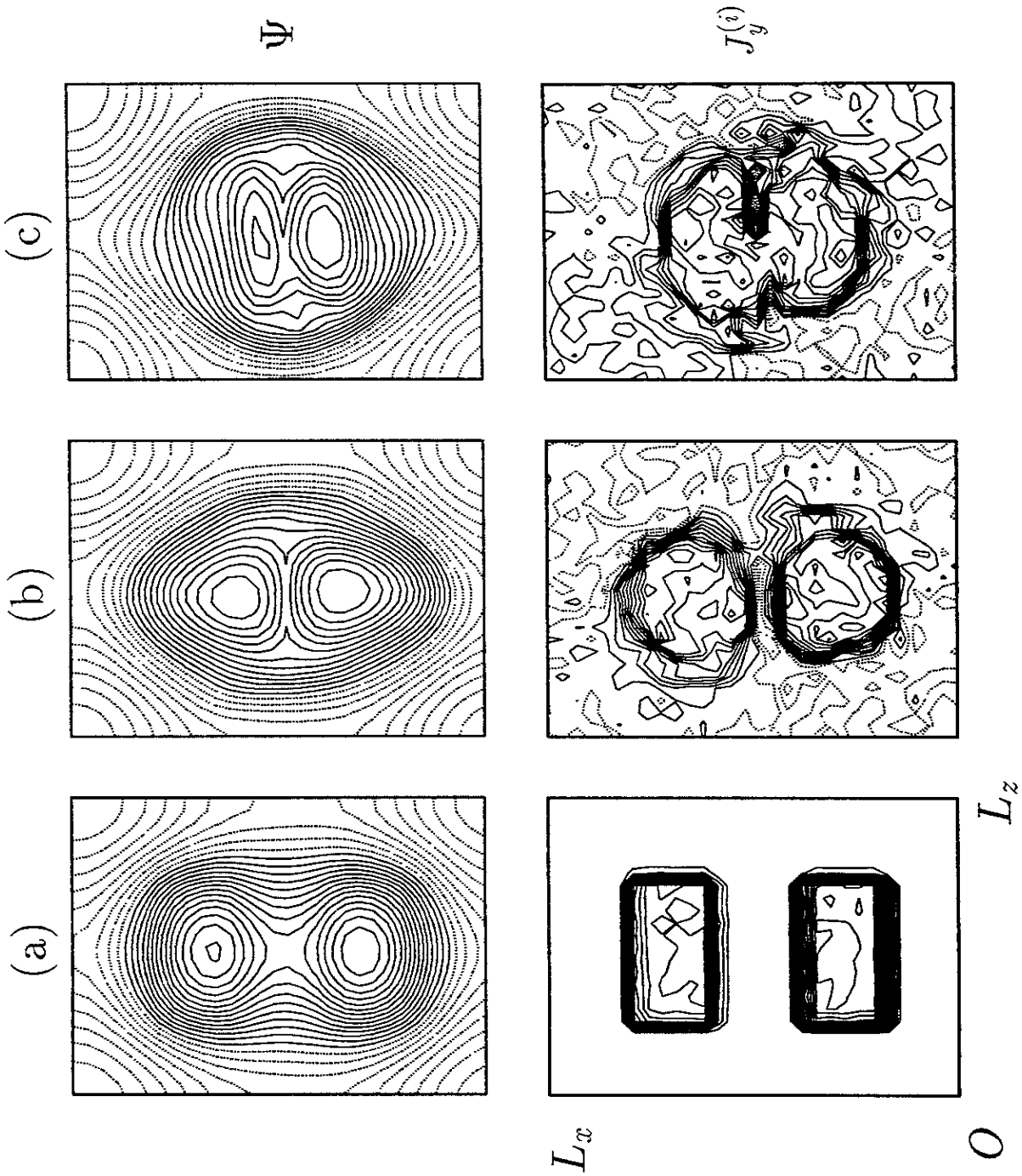

Figure 1.

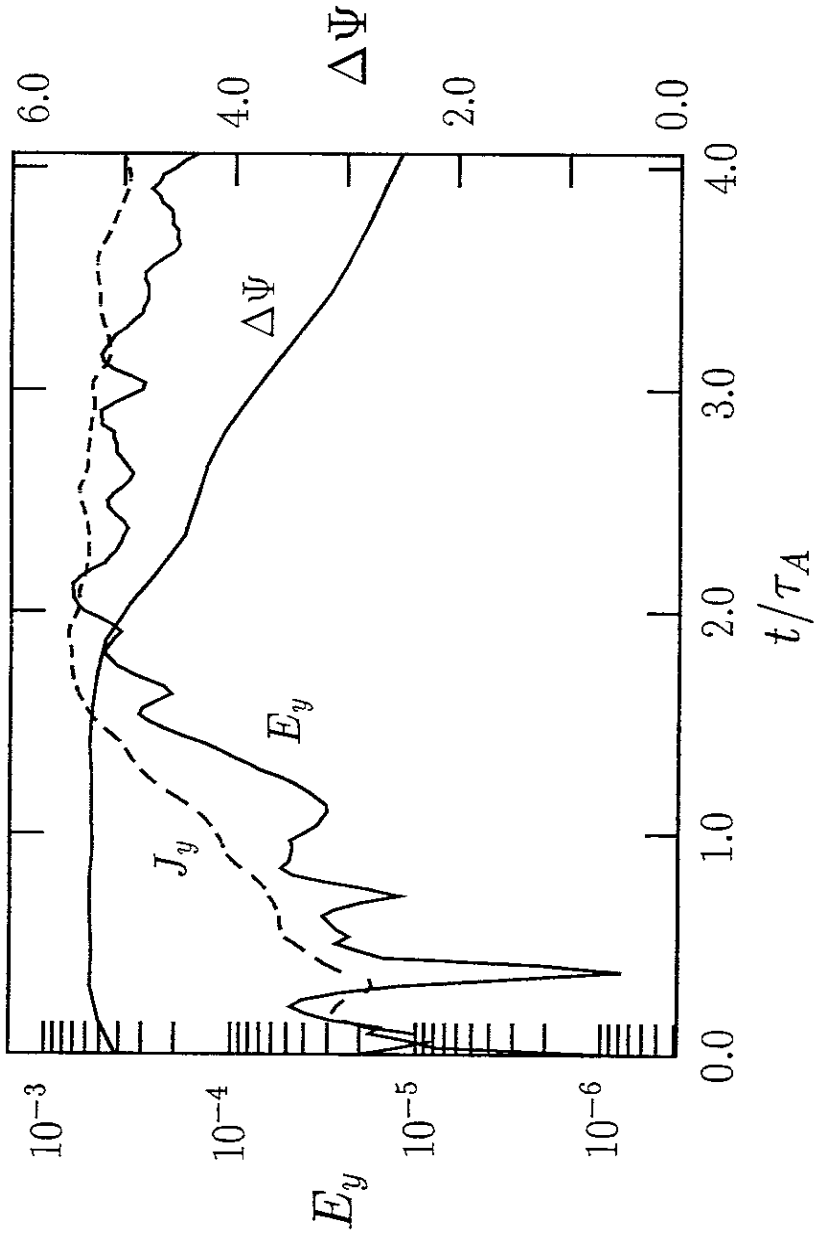
6.0
4.0
2.0
0.0
$\Delta\Psi$
$\Delta\Psi$
E_y
J_y
0.0
1.0
2.0
3.0
4.0
t/τ_A
10^{-3}
10^{-4}
10^{-5}
10^{-6}
E_y

Figure 2.

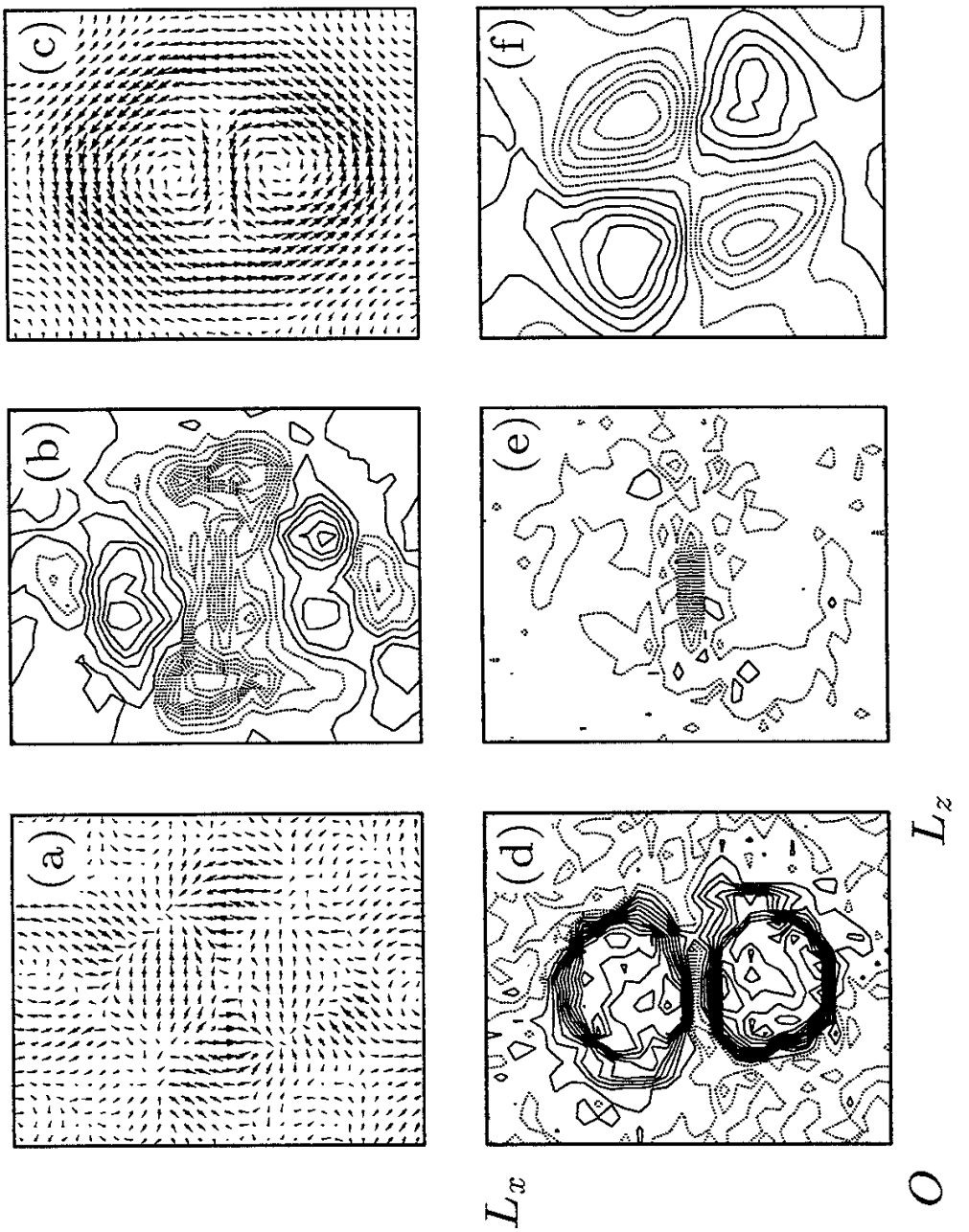

Figure 3.

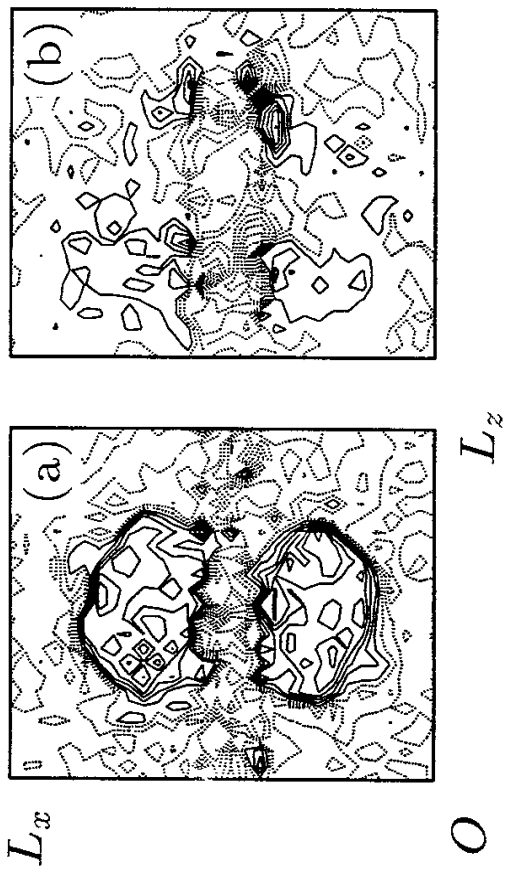

Figure 4.

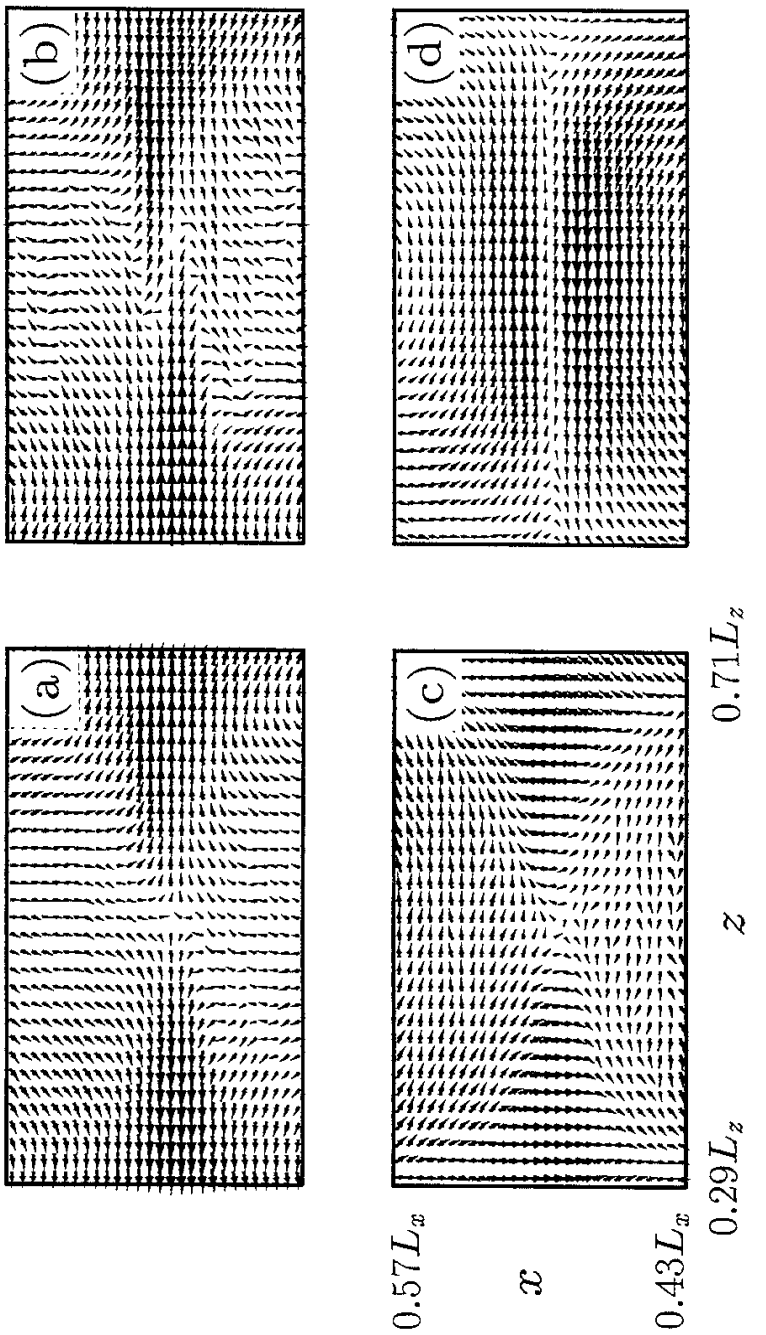

Figure 5.

Recent Issues of NIFS Series

NIFS-227 T. Yamagishi, *Anomalous Cross Field Flux in CHS* ; May 1993

NIFS-228 Y. Ohkouchi, S. Sasaki, S. Takamura, T. Kato, *Effective Emission and Ionization Rate Coefficients of Atomic Carbons in Plasmas;* June 1993

NIFS-229 K. Itoh, M. Yagi, A. Fukuyama, S.-I. Itoh and M. Azumi, *Comment on 'A Mean Field Ohm's Law for Collisionless Plasmas;* June 1993

NIFS-230 H. Idei, K. Ida, H. Sanuki, H. Yamada, H. Iguchi, S. Kubo, R. Akiyama, H. Arimoto, M. Fujiwara, M. Hosokawa, K. Matsuoka, S. Morita, K. Nishimura, K. Ohkubo, S. Okamura, S. Sakakibara, C. Takahashi, Y. Takita, K. Tsumori and I. Yamada, *Transition of Radial Electric Field by Electron Cyclotron Heating in Stellarator Plasmas;* June 1993

NIFS-231 H.J. Gardner and K. Ichiguchi, *Free-Boundary Equilibrium Studies for the Large Helical Device,* June 1993

NIFS-232 K. Itoh, S.-I. Itoh, A. Fukuyama, H. Sanuki and M. Yagi, *Confinement Improvement in H-Mode-Like Plasmas in Helical Systems,* June 1993

NIFS-233 R. Horiuchi and T. Sato, *Collisionless Driven Magnetic Reconnection,* June 1993

NIFS-234 K. Itoh, S.-I. Itoh, A. Fukuyama, M. Yagi and M. *Azumi, Prandtl Number of Toroidal Plasmas;* June 1993

NIFS-235 S. Kawata, S. Kato and S. Kiyokawa , *Screening Constants for Plasma;* June 1993

NIFS-236 A. Fujisawa and Y. Hamada, *Theoretical Study of Cylindrical Energy Analyzers for MeV Range Heavy Ion Beam Probes;* July 1993

NIFS-237 N. Ohyabu, A. Sagara, T. Ono, T. Kawamura and O. Motojima, *Carbon Sheet Pumping;* July 1993

NIFS-238 K. Watanabe, T. Sato and Y. Nakayama, *Q-profile Flattening due to Nonlinear Development of Resistive Kink Mode and Ensuing Fast Crash in Sawtooth Oscillations;* July 1993

NIFS-239 N. Ohyabu, T. Watanabe, Hantao Ji, H. Akao, T. Ono, T. Kawamura, K. Yamazaki, K. Akaishi, N. Inoue, A. Komori, Y. Kubota, N. Noda, A. Sagara, H. Suzuki, O. Motojima, M. Fujiwara, A. Iiyoshi, *LHD Helical Divertor;* July 1993

NIFS-240 Y. Miura, F. Okano, N. Suzuki, M. Mori, K. Hoshino, H. Maeda, T. Takizuka, JFT-2M Group, K. Itoh and S.-I. Itoh, *Ion Heat Pulse after Sawtooth Crash in the JFT-2M Tokamak;* Aug. 1993

NIFS-241 K. Ida, Y.Miura, T. Matsuda, K. Itoh and JFT-2M Group, *Observation of non Diffusive Term of Toroidal Momentum Transport in the JFT-2M Tokamak;* Aug. 1993

NIFS-242 O.J.W.F. Kardaun, S.-I. Itoh, K. Itoh and J.W.P.F. Kardaun, *Discriminant Analysis to Predict the Occurrence of ELMS in H-Mode Discharges;* Aug. 1993

NIFS-243 K. Itoh, S.-I. Itoh, A. Fukuyama, *Modelling of Transport Phenomena;* Sep. 1993

NIFS-244 J. Todoroki, *Averaged Resistive MHD Equations;* Sep. 1993

NIFS-245 M. Tanaka, *The Origin of Collisionless Dissipation in Magnetic Reconnection;* Sep. 1993

NIFS-246 M. Yagi, K. Itoh, S.-I. Itoh, A. Fukuyama and M. Azumi, *Current Diffusive Ballooning Mode in Seecond Stability Region of Tokamaks;* Sep. 1993

NIFS-247 T. Yamagishi, *Trapped Electron Instabilities due to Electron Temperature Gradient and Anomalous Transport;* Oct. 1993

NIFS-248 Y. Kondoh, *Attractors of Dissipative Structure in Three Disspative Fluids;* Oct. 1993

NIFS-249 S. Murakami, M. Okamoto, N. Nakajima, M. Ohnishi, H. Okada, *Monte Carlo Simulation Study of the ICRF Minority Heating in the Large Helical Device;* Oct. 1993

NIFS-250 A. Iiyoshi, H. Momota, O. Motojima, M. Okamoto, S. Sudo, Y. Tomita, S. Yamaguchi, M. Ohnishi, M. Onozuka, C. Uenosono, *Innovative Energy Production in Fusion Reactors*; Oct. 1993

NIFS-251 H. Momota, O. Motojima, M. Okamoto, S. Sudo, Y. Tomita, S. Yamaguchi, A. Iiyoshi, M. Onozuka, M. Ohnishi, C. Uenosono, *Characteristics of D-^{3}He Fueled FRC Reactor: ARTEMIS-L,* Nov. 1993

NIFS-252 Y. Tomita, L.Y. Shu, H. Momota, *Direct Energy Conversion System for D-^{3}He Fusion,* Nov. 1993

NIFS-253 S. Sudo, Y. Tomita, S. Yamaguchi, A. Iiyoshi, H. Momota, O. Motojima, M. Okamoto, M. Ohnishi, M. Onozuka, C. Uenosono,
Hydrogen Production in Fusion Reactors, Nov. 1993

NIFS-254 S. Yamaguchi, A. Iiyoshi, O. Motojima, M. Okamoto, S. Sudo, M. Ohnishi, M. Onozuka, C. Uenosono,
Direct Energy Conversion of Radiation Energy in Fusion Reactor, Nov. 1993

NIFS-255 S. Sudo, M. Kanno, H. Kaneko, S. Saka, T. Shirai, T. Baba,
Proposed High Speed Pellet Injection System "HIPEL" for Large Helical Device
Nov. 1993

NIFS-256 S. Yamada, H. Chikaraishi, S. Tanahashi, T. Mito, K. Takahata, N. Yanagi, M. Sakamoto, A. Nishimura, O. Motojima, J. Yamamoto, Y. Yonenaga, R. Watanabe,
Improvement of a High Current DC Power Supply System for Testing the Large Scaled Superconducting Cables and Magnets; Nov. 1993

NIFS-257 S. Sasaki, Y. Uesugi, S. Takamura, H. Sanuki, K. Kadota,
Temporal Behavior of the Electron Density Profile During Limiter Biasing in the HYBTOK-II Tokamak; Nov. 1993

NIFS-258 K. Yamazaki, H. Kaneko, S. Yamaguchi, K.Y. Watanabe, Y.Taniguchi, O.Motojima, LHD Group,
Design of Central Control System for Large Helical Device (LHD); Nov. 1993

NIFS-259 K. Yamazaki, H. Kaneko, S. Yamaguchi, K.Y. Watanabe, Y.Taniguchi, O.Motojima, LHD Group,
Design of Central Control System for Large Helical Device (LHD); Nov. 1993

NIFS-260 B.V.Kuteev,
Pellet Ablation in Large Helical Device; Nov. 1993

NIFS-261 K. Yamazaki,
Proposal of "MODULAR HELIOTRON': Advanced Modular Helical System Compatible with Closed Helical Divertor; Nov. 1993

NIFS-262 V.D.Pustovitov,
Some Theoretical Problems of Magnetic Diagnostics in Tokamaks and Stellarators; Dec. 1993

NIFS-263 A. Fujisawa, H. Iguchi, Y. Hamada
A Study of Non-Ideal Focus Properties of 30° Parallel Plate Energy Analyzers; Dec. 1993

NIFS-264 K. Masai,
Nonequilibria in Thermal Emission from Supernova Remnants;
Dec. 1993

NIFS-265 K. Masai, K. Nomoto,
X-Ray Enhancement of SN 1987A Due to Interaction with its Ring-like Nebula; Dec. 1993

NIFS-266 J. Uramoto
A Research of Possibility for Negative Muon Production by a Low Energy Electron Beam Accompanying Ion Beam; Dec. 1993

NIFS-267 H. Iguchi, K. Ida, H. Yamada, K. Itoh, S.-I. Itoh, K. Matsuoka, S. Okamura, H. Sanuki, I. Yamada, H. Takenaga, K. Uchino, K. Muraoka,
The Effect of Magnetic Field Configuration on Particle Pinch Velocity in Compact Helical System (CHS); Jan. 1993

NIFS-268 T. Shikama, C. Namba, M. Kosuda, Y. Maeda,
Development of High Time-Resolution Laser Flash Equipment for Thermal Diffusivity Measurements Usting Miniature-Size Specimens; Jan. 1994

NIFS-269 T. Hayashi, T. Sato, P. Merkel, J. Nührenberg, U. Schwenn,
Formation and 'Self-Healing' of Magnetic Islands in Finite-β Helias Equilibria; Jan. 1994

NIFS-270 S. Murakami, M. Okamoto, N. Nakajima, T. Mutoh,
Efficiencies of the ICRF Minority Heating in the CHS and LHD Plasmas; Jan. 1994

NIFS-271 Y. Nejoh, H. Sanuki,
Large Amplitude Langmuir and Ion-Acoustic Waves in a Relativistic Two-Fluid Plasma; Feb. 1994

NIFS-272 A. Fujisawa, H. Iguchi, A. Taniike, M. Sasao, Y. Hamada,
A 6MeV Heavy Ion Beam Probe for the Large Helical Device;
Feb. 1994

NIFS-273 Y. Hamada, A. Nishizawa, Y. Kawasumi, K. Narihara, K. Sato, T. Seki, K. Toi, H. Iguchi, A. Fujisawa, K. Adachi, A. Ejiri, S. Hidekuma, S. Hirokura, K. Ida, J. Koong, K. Kawahata, M. Kojima, R. Kumazawa, H. Kuramoto, R. Liang, H. Sakakita, M. Sasao, K. N. Sato, T. Tsuzuki, J. Xu, I. Yamada, T. Watari, I. Negi,
Measurement of Profiles of the Space Potential in JIPP T-IIU Tokamak Plasmas by Slow Poloidal and Fast Toroidal Sweeps of a Heavy Ion Beam; Feb. 1994